Desalination and Water Treatment
www.deswater.com

doi: 10.5004/dwt.2017.21536

97 (2017) 213–224
November

Synthesis of chitosan-SnO_2 nanoparticles biocomposite for dispersive micro-solid phase extraction of iron in environmental and wastewater samples and its determination by microvolume spectrophotometric detection

Roya Mirzajani*, Nahid Pourreza, Jafar Burromandpiroze

Chemistry Department, College of Sciences, Shahid Chamran University of Ahvaz, Ahvaz, Iran, Tel./Fax: +986113738044; emails: rmirzajani@scu.ac.ir (R. Mirzajani), npourreza@scu.ac.ir (N. Pourreza), jafarburromandpiroze@yahoo.com (J. Burromandpiroze)

Received 7 April 2017; Accepted 5 October 2017

ABSTRACT

In this study, chitosan-SnO_2 nanoparticles biocomposite was synthesized and investigated as an efficient green biosorbent for adsorption of Fe(II) ions. The as-prepared bio-nanocomposite was characterized by Fourier-transform infrared spectroscopy, X-ray powder diffraction spectroscopy, transmission electron microscopy, scanning electron microscopy, and energy dispersive X-ray spectroscopy. Furthermore, a dispersive micro-solid phase extraction (D-μ-SPE) based on microvolume spectrophotometric detection technique was developed for preconcentration as well as determination of Fe(II) ions in environmental and wastewater samples. After reduction of Fe(III) ions by the addition of hydroxylamine hydrochloride as reducing agent, the system was applied to the total iron. Different parameters influencing the extraction efficiency including sample pH, the amount of adsorbent, adsorption time, and properties of desorption solvent were optimized. The adsorption isotherms of the synthesized adsorbent were also studied. The adsorption isotherm was well described by the Freundlich model and showed good adsorption capacity for the Fe(II) ions (17.24 mg g^{-1}). The calibration graph was linear in the range 10–1,200 ng mL^{-1} of Fe(II) and total iron. The detection limit of the method for determination of Fe(II) was 2.8 ng mL^{-1} with a relative standard deviation of less than 1.3%. The adsorption capacity of the regenerated adsorbents was maintained at 90% even after the fourth adsorption–desorption cycle.

Keywords: Chitosan; SnO_2 nanoparticle; Dispersive micro-solid phase extraction; Iron; Microvolume spectrophotometry

1. Introduction

Metals are a natural part of our environment; they are present in all of earth's compartments (air, water, and soil) [1,2]. Many metals, such as iron, zinc, copper, and chrome, fulfill essential functions in every living organism. For all elements essential to life, there exists an optimal dose. If human beings or organisms receive too little of an element, deficiency symptoms can arise. With an overdose, even of useful elements, poisoning can occur. Iron plays an important role in various environmental, industrial, biological, and medical applications [3]. Also, this element is an essential micronutrient for living organisms due to its vital role in electron transport reactions, oxygen transport, and energy metabolism in biological systems. Investigations about iron deficiencies are carried out worldwide [4]. However, in dietary sources, excessively adding iron or inappropriately choosing an iron supplement may cause iron toxicity [5].

These days the impacts of iron as a needed element and pollutant are well established. Iron levels are important for the health of mammals, and iron accumulates in iron deposits in the body as ferritin. Levels below 12 μg L^{-1} indicate a loss of iron, causing anemia [6]. High levels of iron are associated with an increased risk for cancer, heart disease, and other illnesses such as endocrine problems, arthritis, diabetes, and liver disease [7]. Safe limits for iron in drinking water are restricted

* Corresponding author.

to 2.0 mg L^{-1} by the World Health Organization. European Legislation has established a maximum contaminant level of 200 μg L^{-1} for iron [8]. Therefore, it is very important to determine trace amounts of iron in water samples for environmental protection, hydrogeology, and some chemical processes [9].

As a result, low cost and user-friendly analytical methods have become attractive for the determination of trace levels of iron in different kinds of samples. The most common analytical method applied to Fe determination is UV/Vis spectrophotometry [10–12]; however, examples of the application of other techniques such as amperometry, differential pulse voltammetry [3,13], inductively coupled plasma mass spectrometry [14], atomic absorption spectroscopy [8,15–16], and ion chromatography spectrophotometry [17] were also reported. However, the sensitivity and selectivity of most of these methods are usually insufficient for the direct determination of an element at very low concentration levels in complex matrices and real samples. Therefore, a separation/preconcentration step prior to the analysis is usually necessary.

Today, solid phase extraction (SPE) has become the most common sample pretreatment method for preconcentration, matrix simplification, and medium exchange in environmental samples [18]. In SPE, the sorbent utilized is a key factor as the extraction depends on the partition coefficient of analytes between a solid and a liquid phase. Recently, versatile materials have been used as SPE sorbents, and nanomaterials have specifically aroused great interest due to their unique physical properties [19].

Compared with micrometer-sized particles used in SPE, nanoparticles offer a significantly higher surface area to volume ratio and a short diffusion route, resulting in a higher extraction capacity, rapid dynamics of extraction, and higher extraction efficiencies [20]. However, nanoparticles readily form aggregates because of van der Waals forces [21], and this drives the need for energy intensive post-treatment filtration to recover the nanoparticles for regeneration and reuse [22]. To overcome this limitation, it is necessary to embed nanocomposites into a porous matrix. The utilization of this modification has two-fold advantages. First, it can improve the stability and dispersibility. Second, as a hosting material, the separation and reuse of modified nanoparticles from the reaction system become easy [23].

Polymers are frequently used to stabilize or support metal nanoparticles [24]. Generally, the choice of polymer can influence the final efficiency of the adsorbent. The use of biopolymers has been gaining wide attention because of their low cost and high contents of amino and hydroxyl functional groups, which show significant adsorption potential for the adsorption of various heavy metal ions [25]. Among the biomaterials, chitosan has excellent stabilization properties for metal nanoparticles, and it has been regarded as the biopolymer for modification because of its biodegradability, biocompatibility, nontoxicity, and easy availability [26]. Chitosan is a linear polysaccharide based on a glucosamine unit, and it is obtained through chitin deacetylation, which is a major component of crustacean shells and one of the most abundant biopolymers in nature [27].

Several researchers have demonstrated that chitosan can be used as a suitable biopolymer adsorbent for the adsorption of metal ions from aqueous solutions [28]. The presence of amine and hydroxyl groups in the backbone of chitosan chains can serve as coordination and reaction sites, so it can form complexes with metal ions during adsorption processes, depending on the kind of metal ions and the pH of the solution, and this gives high binding capacity to the polymer [29]. The acidic pH of some real samples could severely limit the use of chitosan as an adsorbent in adsorbing dyes and metal ions due to the dissolution tendency of chitosan in an acidic solution [30]. To overcome this problem, a cross-linked agent or immobilization of chitosan on a support surface was used to stabilize chitosan in acidic solutions.

In recent years, chitosan-based metal oxide nanoparticle composites, including zinc oxide, copper oxide, ferric oxides, manganese oxides, aluminum oxides, titanium oxides, magnesium oxides, cerium oxides, and tin oxide [31–36], are identified as promising materials for photocatalytic reactions, degradation of azo dyes, sensors and heavy metal adsorption from aqueous systems. So far, the adsorption of metal ions on chitosan modified SnO_2 nanoparticles has not yet been investigated.

This work describes a simple, rapid, and inexpensive procedure for the preparation of a novel biosorbent via the modification of SnO_2 nanoparticles with chitosan. This biocomposite was further successfully used as an efficient adsorbent for dispersive micro-SPE for the microvolume spectrophotometric determination of Fe(II) ions and the total iron at a nanomolar concentration in environmental and wastewater samples. The results demonstrated herein for the determination of iron has good sensitivity, selectivity, and reproducibility.

2. Experimental setup

2.1. Instruments

The absorbance measurements were done using a PG UV-Vis spectrophotometer model T 80 with quartz cells. Fourier-transform infrared spectroscopy (FTIR) spectra were obtained using a KBr tablet on a FTIR spectrometer spectrum RX1 (Perkin Elmer, Waltham, MA, USA). A pH meter (827 pH lab, Metrohms, Herisau, Switzerland) was used to control the pH of the solution, with a combined glass electrode. The particle morphology and scanning electron microscopy (SEM) analysis were performed by Hitachi S5200 in the scanning mode at 30 kV, 30 lA current. The chemical compositions were determined by an energy dispersive X-ray spectrometer (EDS) attached to the SEM instrument. X-ray powder diffraction (XRD) patterns were recorded on a D8 Advance diffractometer (Bruker, Karlsruhe, Germany) with Cu Kα radiation (40 kV, 40 mA). Data were recorded with a speed of 2° min^{-1} and a step of 0.05°. Transmission electron microscopic (TEM) images were taken using a Zeiss-EM10C at 80 kV. HERMLE bench centrifuge (2206A, Germany) was used to accelerate the phase separation.

2.2. Reagents and solutions

All chemicals used were of analytical grade, and double distilled water was used throughout the experiments. Iron(II) stock solution, 500 mg L^{-1}, was prepared by dissolving 0.878 g of iron(II) ammonium sulphate hexahydrate (Merck, Darmstadt, Germany) in 25 mL of 1.0 mol L^{-1} HCl

and diluted to volume in a 250 mL measuring flask. Iron(III) standard stock solution (500 mg L^{-1}) was prepared by dissolving 1.079 g of $Fe(NH_4)(SO_4)_2.12H_2O$ in 20 mL of 1:1 HCl and diluted to 250 mL with water. Tin oxide nanoparticles (SnO_2-NPs) with an average size of 20–30 nm were purchased from the Neutrino Corporation (Iran). The working standard solutions were freshly prepared by dilution with water. Hydroxylamine hydrochloride, 10% solution (w/v), was prepared by dissolving 10.0 g of hydroxylamine hydrochloride in 100 mL water. The solution was freshly prepared every day. 1,10-phenanthroline (Phen) solution 5×10^{-3} M was prepared by dissolving appropriate amount of 1,10- phenanthroline in 100 mL of 0.05% (v/v) ethanol. The solutions were freshly prepared every day. pH adjustments were performed with both HCl (Merck) and NaOH (Merck) solutions 0.01–1.0 mol L^{-1}. A phosphate buffer (pH 5) was prepared by addition of 0.1 M NaOH to 0.1 M phosphoric acid and adjusting the pH at 5 using a pH meter.

2.3. Preparation of chitosan-SnO_2 nanoparticle biocomposite

In order to prepare the chitosan-SnO_2 nanoparticle (CS–SnO_2 Np) biocomposite, 2 g of chitosan was first dissolved in acetic acid solution (2 wt%) and stirred for 1 h. This solution was added to 1 g of SnO_2 nanoparticle and the reaction mixture was refluxed for 24 h under continuous stirring. The products were washed several times with acetic acid solution (2 wt%) and double distilled water to remove unreacted chitosan. The prepared powder was dried again at 50°C for 12 h, ground and stored in a desiccator prior to the characterizations and utilized in the adsorption tests.

2.4. Water sample preparations

River water sample was collected from Jarahi River (Mahshahr, Iran) and Jarahi River (Mahshahr, Iran). The drinking water samples were collected from tap water in Ahvaz city and the two different kinds of industrial wastewater samples and cooling water were collected from maroon petrochemical industry (Mahshahr, Iran). The water samples were filtered through a 0.45 micropore size membrane filter paper, to remove suspended particulate matter. All the samples were collected in pre-washed brown sampling bottles and stored in 0–4°C until extraction.

2.5. General preconcentration procedure

25 mL of an aqueous sample solution containing an analyte (0.5 μg mL^{-1}) with a pH 5 and 50 mg of biosorbent were placed in a sample vial. The solutions were stirred for 30 min using a magnetic stirrer. Afterwards, the Fe(II) ion loaded biocomposite was separated by centrifuging the above mixture at 3,500 rpm for 3 min. Desorption processes were performed on a loaded biocomposite with 400 μL of a 1,10-phenanthroline solution 5×10^{-3} mol L^{-1}. This method is based on a complex of bivalent iron with 1,10-phenanthroline as an eluent and a compounding agent. It can be used as a visible spectrophotometric signal for the determination of Fe(II) ions after its preconcentration. Lastly, the absorbance intensity was measured using a microcuvette (350 μL) at 525 nm (λ_{max}) against a blank reagent. For the determination of total iron, a 10 mL working solution containing both Fe(II) and Fe(III) ions was placed in a beaker and 5 mL of 10% hydroxylamine hydrochloride solution was added. Iron(III) is reduced quantitatively to iron(II) in the presence of hydroxylamine; the reaction for this reduction is shown below [37]:

$$2HONH_3^+Cl^- + 2Fe^{3+} <===> 4H^+ + 2H_2O + N_2 + 2Fe^{2+} + 2Cl^-$$

when Fe(III) ions are completely reduced to Fe(II) ions, 2 mL of a phosphate buffer solution (pH 5) was added and the solution was diluted to 25 mL. The above procedure was utilized for the preconcentration of iron ions on CS–SnO_2 NPs biocomposites. Then, the desorption process was performed, and the absorbance was measured at 525 nm against a blank reagent. The schematic of the preparation of the CS–SnO_2 NPs biocomposites and their usage for the dispersive micro-SPE of iron ions is presented in Fig. 1.

2.6. Adsorption isotherms studies

In order to evaluate the effect of CS–SnO_2 NP biocomposite adsorbent on the adsorption of Fe(II) ions from aqueous solutions, a known mass of the adsorbent (0.05 g) was equilibrated in 20 mL of Fe(II) sample solutions at concentrations ranging from 5 to 50 mg L^{-1} by shaking for 30 min (the adsorption equilibrium) at a pH 5.0, respectively. Then the concentrations of Fe(II) ions in the supernatant of the solutions were determined.

The amount of Fe(II) ions adsorbed at time t, q_t (mg/g), was calculated by Eq. (1) [38]:

$$q_t = \frac{(C_0 - C_t)V}{W} \tag{1}$$

where C_0 and C_t are initial and equilibrium concentrations in mg/L, W is the dry mass of adsorbent in grams and V is the volume of solution in liters. q_e (mg g^{-1}) which is the amount of adsorbed analyte (mg) per 1 g of the adsorbent at equilibrium time was then calculated using Eq. (2) [39]:

$$q_e = \frac{(C_0 - C_e)V}{W} \tag{2}$$

where C_e is the concentration of Fe(II) ions in solution at equilibrium time.

3. Results and discussion

3.1. Characterization of the adsorbent

Fig. 2(a) shows the FTIR spectra of the unmodified SnO_2 nanoparticles. The band around the 3,394–3,409 cm^{-1} region is due to the stretching vibration of the O–H bond. This band is due to the OH groups and the adsorbed water. The broad band at 1,620–1,630 cm^{-1} is attributed to the bending vibration of water molecules, on the outer surface of SnO_2 nanoparticles. The peak, at 521 cm^{-1}, agrees with the stretching vibrations of the terminal Sn–OH. The absorbance band around at 637 cm^{-1} could be attributed to O–Sn–O, Sn–O, or O–Sn–O lattice [40]. Fig. 2(b) shows the FTIR spectra of

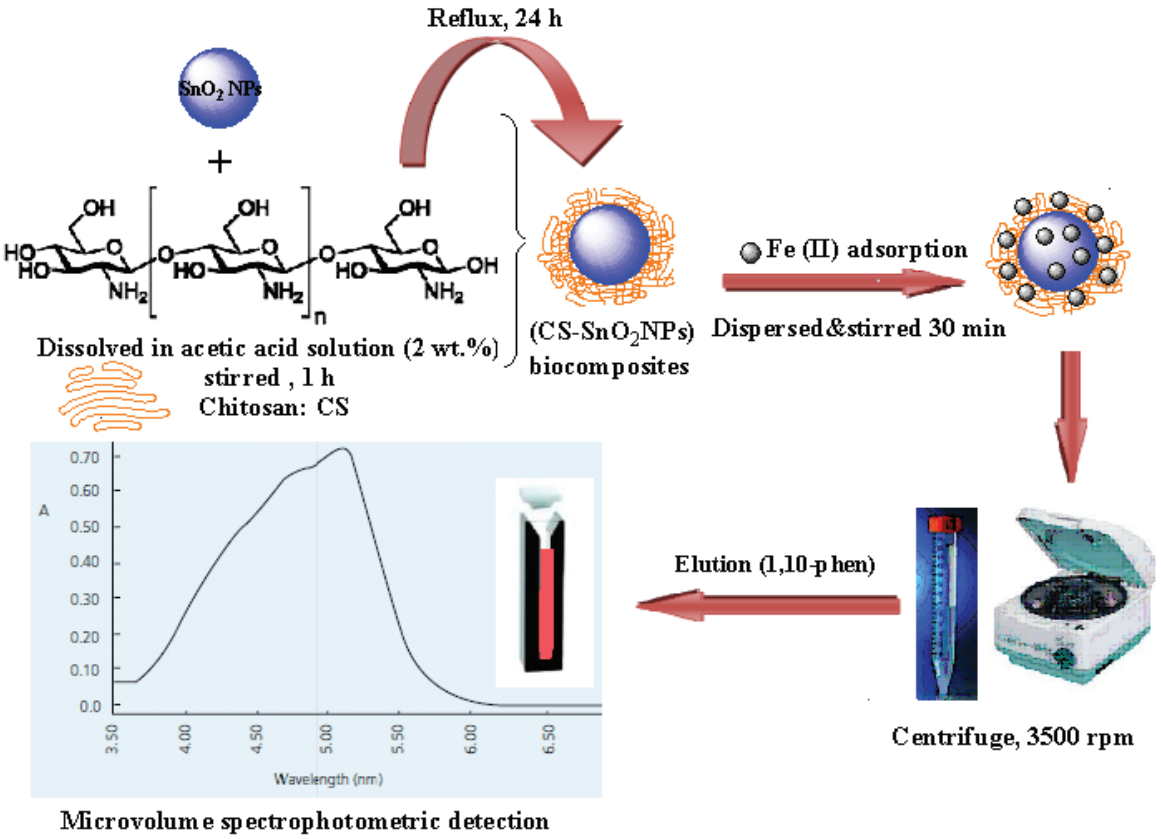

Fig. 1. Schematic preparation process of the CS–SnO_2 NPs biocomposites and their using for the dispersive micro-solid phase extraction of iron ions.

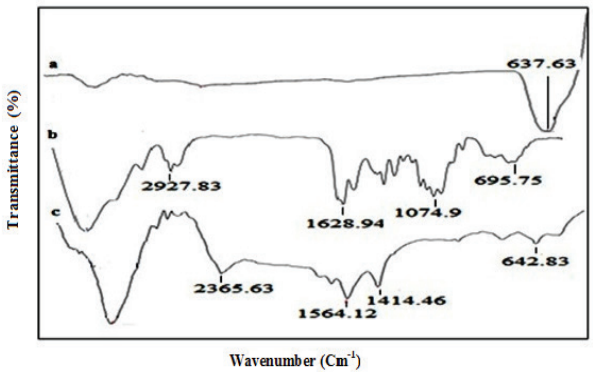

Fig. 2. FTIR spectra of (a) unmodified SnO_2 nanoparticles, (b) chitosan, and (c) CS–SnO_2 NPs biocomposites.

chitosan. Different stretching vibration bands were observed in the range 3,425–2,881 cm^{-1} and they could be assigned to N–H, O–H, and NH_2, which are present in chitosan in different amounts. An absorption peak at 2,928.83 cm^{-1} indicates the presence of a methylene group in CH_2OH and a methine group in a pyranose ring, and the corresponding stretching vibrations of these groups. The absorption band at 1,628.94 cm^{-1} can be due to the scissoring vibration of an NH_2 group present in chitosan. The peaks at 1,074.6 and 1,433.8 cm^{-1} are assigned to the C–N and C–O stretching vibrations. The peak at 695.75 cm^{-1} is a ring stretching, a characteristic bond for a β-1-4 glycosidic linkage [41]. The FTIR spectra of the biocomposite (Fig. 2(c)) show the characteristic infrared band at 642.83 cm^{-1}, which could be contributed to the metal oxygen stretching vibration of the composite and it indicates the presence of a thin oxide nanoparticle vibration. The absorption band at 1,414.46 cm^{-1} could be assigned to –C–O stretching of the primary alcoholic group in chitosan. The broad adsorption peak, near 3,300–3,500 cm^{-1}, was attributed to the stretching vibration of O–H, the extension vibration of N–H, and the inter hydrogen bonds of the polysaccharide. These results confirm that the chitosan polymer was successfully coated on the SnO_2 nanoparticles.

The XRD pattern of the biocomposite product is shown in Fig. 3(a). Intense peaks at 2θ values of 26.3, 33.6, 37.8, 51.5, 54.5, 57.5, 61.7, 64.5, 70.9, 78.5 (values in A°), and all the prominent planes (110, 101, 200, 211, 220, 002, 310, 301, 321) were observed. All the peaks were matched with diffraction data of the tetragonal structure of tin oxide (JCPDS 00-001-0625) and the position of the main peak is 2θ = 26.3. The observed diffraction peaks are quite similar to those of the unmodified SnO_2 nanoparticles (Fig. 3(b)) [42]. Hence, X-ray diffraction analysis confirms the crystalline nature of the synthesized CS–SnO_2 NPs biocomposites and also shows that the crystalline structure of SnO_2 NPs was retained even after treatment. No intense impurity diffraction peaks were observed, indicating the high purity of the final products.

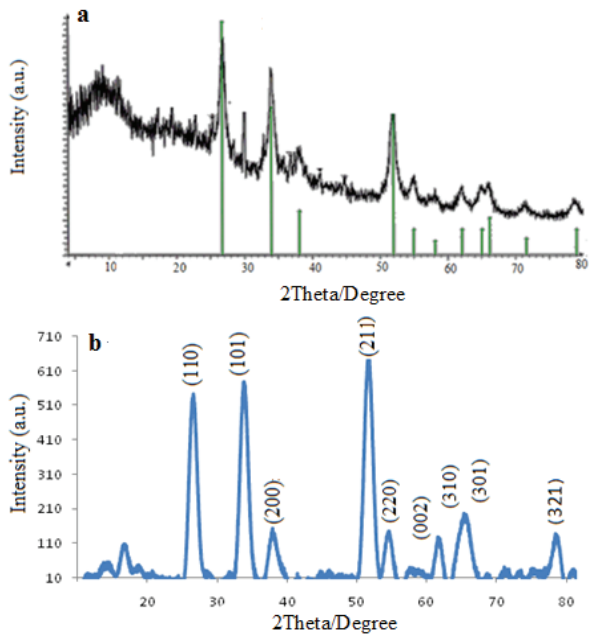

Fig. 3. (a) The X-ray diffraction pattern for CS–SnO_2 NPs biocomposites, (b) the X-ray diffraction pattern for unmodified SnO_2 nanoparticles.

Figs. 4(a) and (b) show SEM images of the tin oxide nanoparticles before surface modification. The nanoparticles have spherical morphologies with sizes smaller than 50 nm. Figs. 4(c) and (d) show TEM images of the CS–SnO_2 NP biocomposite. As shown in the figure, the porous structure of the biocomposite enables the adsorbent to show the high adsorption capacity. The adsorbent particles were nano-sized and spheroidal in morphology. The presence of SnO_2 nanoparticle in the center and a coating of chitosan in the outer layer are also observed.

Elemental analysis of CS–SnO_2 NP biocomposite was studied by energy dispersive X-ray as shown in Fig. 5. As illustrated in this figure elemental characteristic peaks of Sn, O, C, and N were detected which confirmed the surface modification process.

3.2. Optimization of conditions

The experimental procedure was optimized to achieve the best chemical conditions for the retention and desorption of the Fe(II) ions. The adsorbed Fe(II) ions were eluted with a 1,10-phenanthroline solution, and the absorbance of the colored complex was measured at 525 nm. A blank solution was also run under similar analytical conditions without adding any Fe(II) ions.

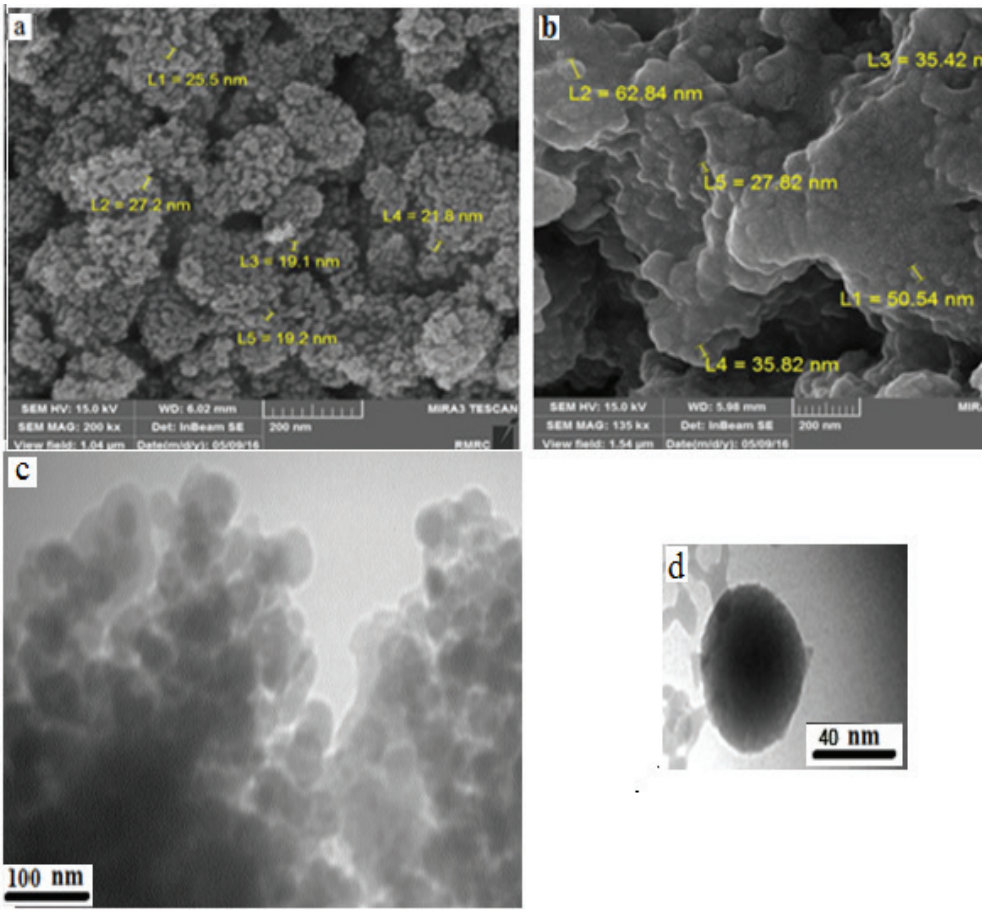

Fig. 4. SEM images of tin oxide nanoparticles (a) before surface modification, (b) after surface modification (CS–SnO_2 NPs biocomposites), and ((c) and (d)) TEM micrographs of chitosan-SnO_2 nanoparticle biocomposite.

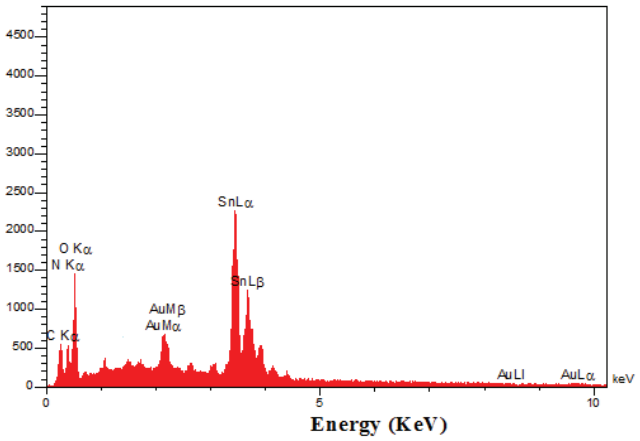

Fig. 5. The EDX image of chitosan-SnO_2 nanoparticle biocomposite (Au signal is related to Au sputtering; the samples were sputter-coated with a 20–30 nm gold layer as the energy dispersive X-ray spectrometer analysis was carried out in a scanning electron microscope).

3.2.1. Effect of pH

It is known that a medium pH can influence the iron adsorption process because it controls the solubility of metals as well as the dissociation state of some functional groups, such as hydroxyl and amino, on the adsorbent surface [43]. The influence of the pH of the sample solution upon the Fe(II) ion adsorption on the CS–SnO_2 NP adsorbent biocomposite was studied. For this purpose, the pH value of a set of solutions (20 mL) each containing 0.5 μg mL^{-1} of Fe(II) ions was adjusted in the range of 2–8 using diluted solutions of 0.1 M HCl or 0.1 M NaOH. The solutions were stirred for 30 min using a magnetic stirrer. Afterwards, the Fe(II) ion loaded biocomposite was separated by centrifuging the mixture at 3,500 rpm for 3 min. The desorption process was performed on a loaded biocomposite with 400 μL of 1,10-phenanthroline solution 5×10^{-3} mol L^{-1}. The results shown in Fig. 6(a) demonstrate that an increase in adsorption is observed up to a pH 5 while it decreased at higher pH values. Therefore, a pH 5 was selected as the optimum for future experiments. The lower uptake in a higher acidic medium may be attributed to the

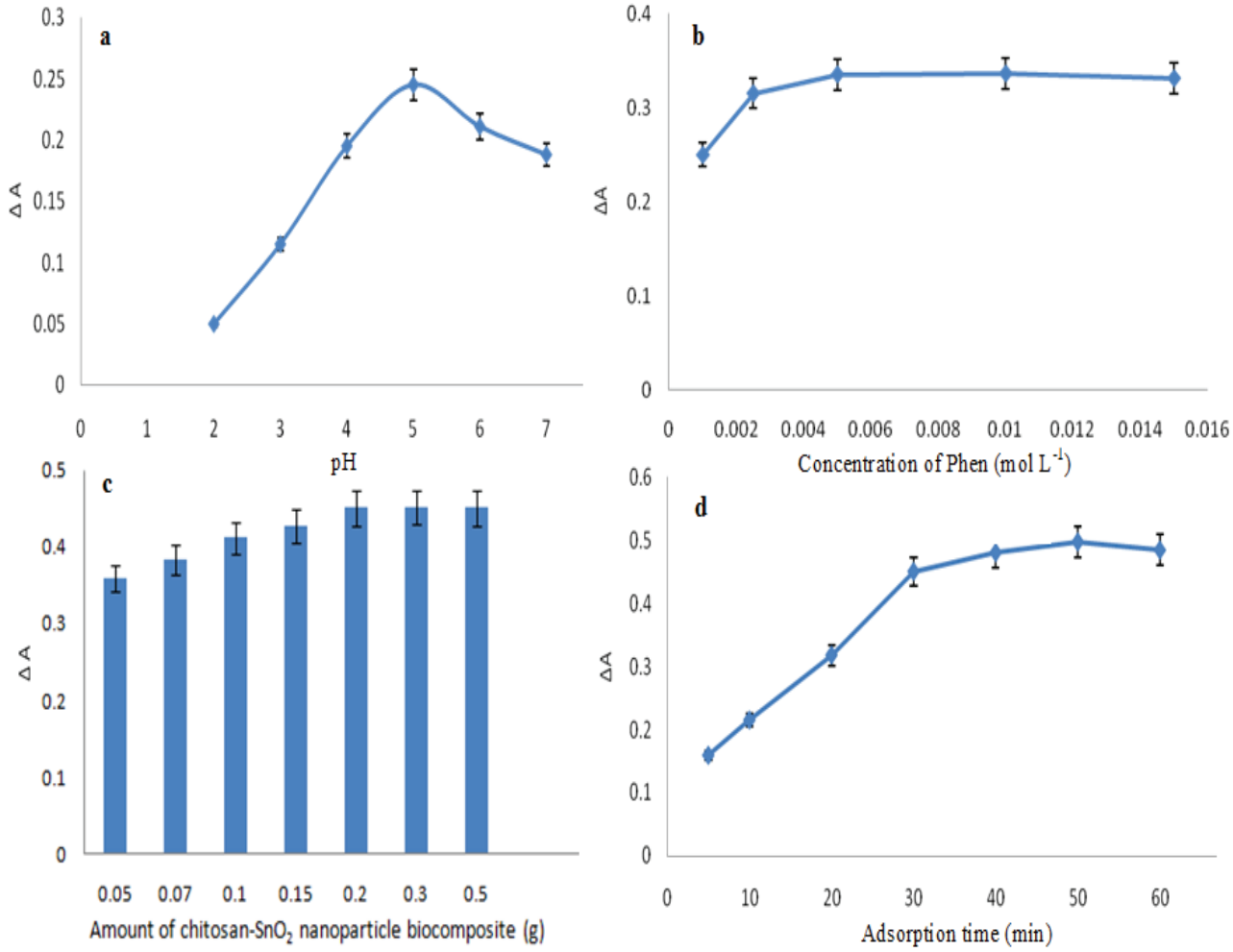

Fig. 6. (a) Effect of pH on the adsorption of 0.5 μg mL^{-1} of Fe(II) ions on the CS–SnO_2 NPs biocomposites (data are for three replicates); (b) effect of Phen concentration for eluting the Fe(II) ions (0.5 μg mL^{-1}) from the biocomposite surface; (c) effect of adsorbent dosage on the adsorption of Fe(II) ions (0.5 μg mL^{-1}); (d) effect of contact time at various time intervals by a fixed amount of the adsorbent (0.2 g). (All data are for three replicates, $n = 3$.)

partial protonation of the active groups of the biosorbent and the competition of H_3O^+ ions in the solution for the adsorption sites of SnO_2 nanoparticle biocomposites. With increasing the pH values to a mildly acidic pH, the surface positive charge on the sorbent decreases, which lowers the coulombic repulsion for the adsorbing iron ions [44]. The observed decrease in the sorption of the iron ions at a pH higher than 5 can be explained on the basis of the formation of different iron species with lower sorption affinities [45]. Extraction was carried out in different types of buffer solutions. A phosphate buffer solution of 2 mL phosphate buffer pH 5 added to 20 mL solutions to maintain this pH was found to be the optimum one, giving the highest absorbance.

3.2.2. Desorption of the adsorbed ions

The volume of eluent was optimized carefully since the use of excess eluent may lead to decrease in the sensitivity and the preconcentration factor. On the other hand, lower amount of eluent compared with the optimum value would result in complete desorption of the analyte from the adsorbent. Hence, desorption of the extracted iron ions was carried out with 1,10-phenanthroline in acidic, alkaline, and ethanolic media (data not shown). Among the different solutions tested, the best recoveries were achieved using an ethanolic solution of 1,10-phenanthroline (Phen) as an extracting solvent and complexing agent. The Phen concentration was also optimized as shown in Fig. 6(b). According to the obtained results, the Phen concentration of 0.005 mol L^{-1} in 5% (v/v) ethanol was identified as the most suitable solvent for eluting the Fe(II) ions from the biocomposite surface. Finally, the effect of volume of the desorption ligand on the Fe(II) desorption and absorbance of complex was studied in the range of 200–2,000 μL. 400 μL of the complexing agent was found to be adequate for the desorption of the retained Fe(II) ions from the biosorbent surface.

3.2.3. Effect of the amount of adsorbent

Every individual particle of the biocomposite has a limited capacity to retain the target molecules [46]. While the extraction may not be completed with insufficient sorbents, an excess of the adsorbents may result in wastage. Different amounts of the biocomposites (between 0.05 and 0.5 g) were analyzed keeping the other parameters fixed. Results in Fig. 6(c) clearly show an increase in absorbance with increase in the amount of adsorbent used and the absorbance of the extracted complex was not considerably increased when more than 0.15 g of the biocomposites was used. Hence, in the following experiments 0.15 g of the nanobiocomposite was utilized to ensure the complete adsorption of the analyte.

3.2.4. Effect of the sample volume

The effect of sample solution volume on the adsorption of Fe(II) was studied by using different sample volumes in the range of 20–250 mL, containing equal amount of Fe(II) at pH 5. Adsorption and desorption processes were performed in the above cases under the optimum conditions using 0.15 g of CS–SnO_2 NP biocomposite as described in the experimental section. The sample volume determines the maximum volume of the water sample that can be introduced into the surface of the adsorbent. The value of this volume is a function of the retention of the analyte on the particular adsorbent, and it can only be altered by a change of adsorbent and is dependent on the parameters such as adsorbent amounts and bed thickness. The results showed that the iron ions present in volumes up to 100 mL were completely and quantitatively adsorbed with synthesized biocomposite. The adsorption then decreased at higher volumes. Therefore, for the determination of trace quantities of Fe(II) ions in samples, a sample volume of 100 mL was selected in order to increase the preconcentration factor. Hence, for 100 mL of sample volume a preconcentration factor of 250 could easily be obtained using 400 μL of desorption agent.

3.2.5. Effect of contact time

The time of contact of the adsorbate and adsorbent plays a significant role for the adsorption of an analyte from an aqueous solution during batch experimental studies. It is helpful in understanding the amount of an analyte adsorbed at various time intervals by a fixed amount of the adsorbent. In this section, 0.2 g of CS–SnO_2 NPs biocomposite adsorbent was used in 20 mL of Fe(II) ions solution, 5 mg L^{-1} at pH 5, with varying times from 5 to 60 min. From Fig. 6(d), it is found that there is a consistent increase in the amount of adsorption up to 30 min, and the adsorption equilibrium is attained after 30 min of contact time. After the equilibrium time, the rate of adsorption decreased and saturation was attained due to the lack of available adsorption sites for the Fe(II) ions. As a result, an agitation time of 30 min was selected for further studies.

3.3. Adsorption isotherms and adsorption capacity

The adsorption isotherms that describe the adsorption equilibrium between the Fe(II) ions on the CS–SnO_2 NP biocomposite and the residual metal ions in the solution during the surface adsorption were studied. Adsorption describes how solutes interact with adsorbents and its parameters are dependent on the surface properties and affinity of the sorbent at a particular temperature. Adsorption isotherms derived using the optimized use of such adsorbents could give important information about the mechanism of adsorption and thus help to design new and efficient adsorbing systems. The adsorption capacity is an important factor as it determines how much sorbent is required for quantitative preconcentration of an analyte from a given solution [47]. When all of the adsorption sites had been occupied by the adsorbed metal ions, the adsorption capacities showed no further visible changes. Studies of the effect of adsorption on the CS–SnO_2 NP biocomposite revealed that a 30-min contact time was adequate for the system to reach equilibrium. Therefore, 0.05 g of the adsorbent was equilibrated in 20 mL of Fe(II) ion sample solutions at concentrations ranging from 5 to 50 mg L^{-1} by shaking for 30 min at a pH 5.0 and the concentration of the unadsorbed iron solution was quantified. The adsorption data obtained was fitted into the general isotherm plots. Three well-known mathematical models (Langmuir, Freundlich, and Dubinin and Radushkevich [D–R]) were used to analyze the adsorption isotherm results.

The Langmuir model is based on the assumption of a structurally homogeneous adsorbent, where all of the adsorption sites are identical and energetically equivalent. This isotherm is given as Eq. (3) [48]:

$$\frac{C_e}{q_e} = \frac{1}{q_{\max}} K_L + \frac{C_e}{q_{\max}} \tag{3}$$

where q_e is the equilibrium concentration of the target on the adsorbent (mg g^{-1}), q_{max} is the monolayer adsorption capacity of the adsorbent (mg g^{-1}), K_L is the Langmuir adsorption constant. The plot of C_e/q_e vs. C_e gives a straight line and the values of q_{max} and K_L can be calculated from the slope and the intercept of the plot, respectively (Fig. 7(a)).

The essential feature of the Langmuir isotherm can be expressed in terms of a dimensionless constant separation factor (R_L) [49]. The R_L value is given by the following equation:

$$R_L = \frac{1}{1 + K_L C_0} \tag{4}$$

K_L is the Langmuir adsorption constant. The degree of suitability of the adsorbent toward the metal ions was estimated from the values of separation factor, which has always been used to indicate whether the adsorption is favorable or not.

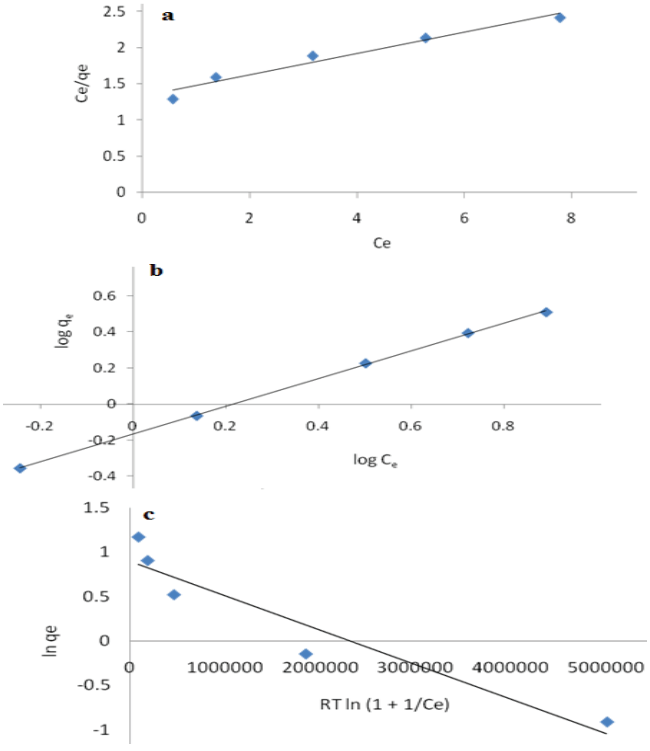

Fig. 7. (a) Langmuir adsorption isotherm of Fe(II) ions on the CS–SnO_2 NPs biocomposites; (b) Freundlich adsorption isotherm of Fe(II) ions on the CS–SnO_2 NPs biocomposites; (c) Dubinin and Radushkevich adsorption isotherm of Fe(II) ions on the CS–SnO_2 NPs biocomposites.

R_L values within the range of $0 < R_L < 1$ indicate a favorable adsorption [50]. In this study, the R_L values of the CS–SnO_2 NP biocomposite adsorbent for Fe(II) ions were in the range of 0.022–0.0027, indicating a favorable adsorption.

The Freundlich equation (Fig. 7(b)) is derived to model the multilayer adsorption and it is valuable in finding the sorption phenomenon with a heterogenous sorbent media. In general, it describes adsorption on an energetically heterogeneous surface for which the adsorbed molecules may be interactive [51]. The Freundlich isotherm is derived from the assumption that the sorption sites are disseminated exponentially with respect to the heat of the sorption model. The linearized form of the Freundlich isotherm is expressed by the following equation [52]:

$$\log q_e = \log K_F + \frac{1}{n} \log C_e \tag{5}$$

where K_F (mg g^{-1}) and n are the Freundlich adsorption isotherm constants and they indicate the extent of adsorption and the degree of nonlinearity of adsorption. The Langmuir and Freundlich isotherms are deficient to clarify the physical and chemical characteristics of adsorption.

However, the D–R isotherm is more general compared with the Langmuir isotherm because it does not assume a homogeneous surface or constant sorption potential. This isotherm model was chosen to estimate the characteristic porosity of the biomass and the apparent energy of adsorption. The D–R equation is shown in Eq. (6) [53]:

$$\ln q_e = \ln q_D - B_D [RT \ln\left(1 + \frac{1}{C_e}\right)]^2 \tag{6}$$

where q_e is the amount of the adsorbed heavy metal per unit adsorbent (mg g^{-1}), and B_D is related to the free energy of sorption per mole of the sorbate as it migrates to the surface of the biomass from infinite distance in the solution and q_D is the D–R isotherm constant related to the degree of sorbate sorption by the sorbent surface [54].

In this equation, R is gas constant (kJ K^{-1} mol^{-1}) and T is temperature (K). A plot of $\ln q_e$ against $(RT \ln[1 + 1/C_e])^2$ for modified sorbents yielded straight lines indicating a good fit of the isotherm to the experimental data (Fig. 7(c)). The apparent energy (E_D) of adsorption from the D–R model can be computed using Eq. (7):

$$E_D = \frac{1}{\sqrt{2B_{DR}}} \tag{7}$$

The sorption energy E_D (kJ mol^{-1}) gives information about the physical and chemical characteristics of adsorption. When the magnitude of E_D is between 8 and 16 kJ mol^{-1}, the sorption process is a chemical ion-exchange and for values of $E_D < 8$ kJ mol^{-1}, the sorption process is physical in nature [55].

Table 1 shows the values of corresponding isotherm parameters, their correlation coefficients (R^2) and related standard errors (SE) for each parameter [56].

Table 1
The Langmuir, Freundlich, and Dubinin–Radushkevich parameters for adsorption of Fe(II) onto CS–SnO_2 NPs biocomposites adsorbent

	q_{max} (mg g^{-1})	K_L (L mg^{-1})	R^2_L	K_F (L mg^{-1})	n	R^2_F	q_D (mg g^{-1})	E (kJ/mol)	R^2_{D-R}
Langmuir	17.24	8.99	0.9598	–	–	–	–	–	–
Freundlich	–	–	–	1.71	2.31	0.9998			
Dubinin–Radushkevich (D–R)	–	–	–	–	–	–	3.50	1.2	0.9091
SE	4.23	3.54	–	0.80	1.15	–	4.80	4.73	–

Fitting the three adsorption models with the experimental data revealed that the Freundlich isotherm is more acceptable than Langmuir isotherms (R^2 = 0.9598) and fits better with experimental data. The correlation coefficients (R^2) of the linear form of the Freundlich model were equal to 0.9998. The values of SE for each parameter obtained in Freundlich isotherm model are correspondingly lower than that of the other two models. These suggest that Freundlich model can generate a satisfactory fit to the experimental data, while both Langmuir isotherm model and the D–R isotherm model cannot. The applicability of the Freundlich isotherm model explains the surface heterogeneity and multilayer coverage of the Fe(II) ions on the surface of CS–SnO_2 NP biocomposite. The n and K_F adsorption level was determined from the Freundlich isotherm. Values of $2 < n < 10$, $1 < n < 2$, and $n < 1$ show good, difficult, and poor adsorption characteristics, respectively [57]. In the cases examined, the value of n for the adsorption of iron ions on the biocomposite adsorbent was 2.31, which is settled between 2 and 10, thus showing good adsorption characteristics and indicating that Fe(II) ions could easily be adsorbed by the adsorbent and this CS–SnO_2 NPs biocomposite adsorbent material exhibit a high adsorption capacity for the target Fe(II) ions. The high K_F value also suggests that the Fe(II) ions are favorably adsorbed on the CS–SnO_2 nanoparticles biocomposite, and thus would allow the easy separation of the analyte from the aqueous solutions.

According to the D–R isotherm, the calculated adsorption energy values, E_D, obtained in this study are below the values of a typical ion-exchange process (1.2 kJ mol^{-1}) suggesting that the adsorption mechanism is a combination of electrostatic interaction and physical sorption. The maximum adsorption capacity for the adsorption of Fe(II) ions on the CS–SnO_2 NPs biocomposite was 17.24 mg g^{-1} based on the Langmuir model. This parameter has been listed in Table 1, together with the literature values of q_{max} for other Fe(II) adsorbents.

3.4. Stability and reusability of the adsorbent

The stability and potential CS–SnO_2 NP biocomposites were investigated to find the reusability and stability of the synthesized sorbent. The solid sorbent was reused at optimum experimental conditions for the separation and preconcentration of Fe(II) ions from various aqueous samples. The adsorbent can be reused after regenerated with 2 mL of pure ethanol and 15 mL distilled water, respectively. The obtained results showed that the biocomposites can be reused for least four adsorption–desorption cycles without any decrease in their efficiency. The sorbent was found to be stable for at least 6 months.

3.5. Analytical performance

In order to validate the proposed method, the analytical features of the method such as linear range of the calibration curve, limit of detection (LOD), limit of quantification (LOQ), accuracy, and precision were measured. The calibration curves were made at the optimal conditions for the Fe(II) ions and total iron. They were constructed by plotting the intensity of the signal acquired using microvolume spectrophotometric method as a function of the Fe(II) ions and total iron concentration and the following linear calibration equations were obtained in the range of 10–1,200 ng mL^{-1}.

The equations are $A_1 = 0.0014\ C_{Fe(II)} - 0.008$ and $A_2 = 0.0014\ C_{total\ iron} - 0.0141$ for the Fe(II) ions and total iron, respectively, where A is the absorbance and C is the concentration of Fe(II) ions and total iron in ng mL^{-1}. The regression coefficient for the lines was higher than 0.9998 which indicated the good linearity and applicability of the method for the quantification of iron ions.

The LOD of the present study for determination of Fe(II) ions was calculated under optimal experimental conditions after application of the preconcentration procedure to blank solutions. An LOD and LOQ values of 2.8 and 9.3 ng mL^{-1}, respectively, were determined based on a signal-to-noise ratio of 3:1 and 10:1, respectively. In order to assess the repeatability of the method, seven replicate determinations were carried out at two concentration levels (50 and 700 ng mL^{-1}), and the relative standard deviations (RSD) were calculated. The RSD for determination of 50 and 700 μg mL^{-1} of Fe(II) ion solutions for seven replicates were 1.3% and 1.1%, respectively (Table 2).

3.6. Effect of foreign ions

The analytical sensitivity and sampling efficiency during the sampling of analytes are related to the extraction selectivity of the adsorbent. In this study, the extraction performance of CS–SnO_2 NPs biocomposites was investigated via the extraction of a series of typical ions including cations and anions. All the extraction processes were performed under the optimal conditions for constant amount of iron(II) with different amounts of diverse ions. Any deviation of ±5% or more from the absorbance value of the standard solution was selected as interference. The results showed that most of the ions used such as Na^+, Ca^{2+}, Mg^{2+}, SO_4^{2-}, NO_3^-, K^+, Al^{3+}, Cl^-, I^- (500 fold), CO_3^{2-}, F^-, Cu^{2+}, Mn^{2+}, Ni^{2+} and Cr^{6+}, Cd^{2+}, Cr^{3+}(250 fold) did not have a considerable effect on the determination of Fe(III) ions.

3.7. Analysis of total iron in real samples

The efficiency of the developed method was further demonstrated by the determination of total iron in various other real water samples such as tap water, two different river water samples, cooling water of a petrochemical company, and two different industrial wastewater samples with satisfactory results (Table 2). The final concentrations of the analyte in the water samples are the average values of consecutive analysis for three times. Furthermore, to evaluate the reliability of the proposed method in real samples, spiked recovery experiments were also carried out.

The extraction recovery (R, %) of Fe(II) ions was calculated from the following equation [58]:

$$\text{Recovery}(\%) = \frac{(C_F - C_A)}{C_S} \times 100 \quad (8)$$

where C_F, C_A, and C_S are the concentrations of the Fe(II) ions found after spiking a specific amount of standard in the real samples, the actual amount of iron ions in the real sample and the concentration of the known amount of the standard that has been spiked to the real sample, respectively.

Table 2
Determination of total iron in water and wastewater samples

Sample	Added (ng mL^{-1})	Found (ng mL^{-1})	Recovery (%)
Tap water	0	0	–
	50	51	102.0
	500	496	99.2
	900	889	98.7
Jarahi river water	0	700	–
	50	748	96.0
	500	1,180	96.0
	900	1,588	98.6
Cooling water	0	104	–
	50	152	96.0
	500	598	98.8
	900	977	97.0
Petrochemical wastewater (1)	0	174	–
	50	225	102.0
	500	667	98.6
	900	1,059	98.3
Petrochemical wastewater (2)	0	1,000	–
	50	1,051	102.0
	500	1,491	98.2
	900	1,928	103.1

Table 2 illustrates the results of real samples spiked with 50, 500, and 900 μg L^{-1} levels of Fe(II) ions. As shown in the table, the recoveries were between 96.0% and 103.1% in all cases demonstrating that the complex real sample matrix had insignificant effects on the extraction efficiency of the CS–SnO_2 NPs biocomposites. From these results, it is obvious that the use of CS–SnO_2 NPs biocomposite in combination with dispersive micro-SPE technique and microvolume spectrophotometry has great potential in the application for extraction of Fe(II) ions in real samples.

3.8. Comparison of this process with other methods

A comparison between the performance of the proposed method with other reported SPE-based methods coupled with various detection techniques is summarized in Table 3. These data clearly indicate that the dispersive micro-SPE technique combined with the microvolume spectrophotometry procedure using CS–SnO_2 NPs biocomposite as adsorbent described herein is a simple, rapid, reliable, and environmentally friendly technique for the selective preconcentration

Table 3
Comparison of proposed method with other pre-treatment methods for the preconcentration of Fe(II) and total iron

Method	PF	LR (ng mL^{-1})	LOD (ng mL^{-1})	RSD (%)	Ref.
FI-SPE/UV-Vis[a]	36	50–500	18.0	3.1	[6]
SPE-FAA[b]	200	2.5–50	0.7	3.2	[8]
SPE/UV-Vis[c]	–	20–450	1.9	3.6	[9]
SPE/UV-Vis[d]	86	200–1,000 nmolL^{1}	5 nmolL^{-1}	4–3	[11]
CPE/UV-Vis[e]	20	25–200	1	–	[16]
DLLME[f]	10	5–400	1.5	1.37	[59]
D-μ-SPE-UV-Vis[g]	250	10–1,200	2.8	<1.3	This work

PF: Preconcentration factor; LR: Linear range; LOD: Limit of detection; RSD: Relative standard deviation.
[a]Flow injection solid phase extraction/ ultraviolet-visible spectrophotometry.
[b]Solid phase extraction/ flame atomic absorption.
[c]Solid phase extraction/ ultraviolet-visible spectrophotometry
[d]Solid phase extraction/ ultraviolet-visible spectrophotometry.
[e]Cloud point extraction / ultraviolet-visible spectrophotometry.
[f]Dispersive liquid -liquid microextraction.
[g]Dispersive micro-solid phase extraction -ultraviolet-visible spectrophotometry.

and sensitive analysis of Fe(II) ions and total iron ions in industrial waste and real water samples. Also, the analytical figures of merit for our proposed method are comparable or better than those previously reported [6,8–9,11,16,59] (Table 3). Our method can also present good quantification extraction efficiency, a wide linear range, and better reproducibility in comparison with the other techniques.

4. Conclusion

In this study, a nanobiocomposite adsorbent based on the modification of SnO_2 nanoparticles with chitosan is used as an extractant for the first time. Dispersive micro-SPE by this inorganic/organic-based bioadsorbent provided a simple, sensitive, selective, and cheap method for simultaneous preconcentration and determination of Fe(II) ions and total iron from complex matrices. An excellent preconcentration performance, sensitive, simple, and cost-effective operation and the lack of consumption of organic toxic solvents exhibited by the CS–SnO_2 NPs biocomposites were a few of the merits of this green adsorbent. This environmentally friendly analytical methodology had a high tolerance to the coexisting ions in real samples and was a well alternative for the determination of Fe(II) and total iron. The results indicated that the adsorption data fitted well to the Freundlich isotherm rather than the Langmuir isotherm. The R_L value showed that the biocomposites were favorable for the adsorption of Fe(II) ions. The performance of this hybrid bioadsorbent in the extraction of iron ions from different matrices was excellent. The CS–SnO_2 NPs biocomposites showed very good reproducibility and reusability. Under the optimal extraction conditions, the developed method provided lower limits of detection, good linearity, good selectivity, and repeatability. Accordingly, this method possesses great potential in the routine analysis of trace of iron ions in real sample.

Acknowledgment

The authors greatly appreciate the financial support of this work by Shahid Chamran University of Ahvaz Research Council.

References

[1] M.L. Inamuddin, Ion Exchange Technology II: Applications, Springer, Netherlands, 2012.
[2] H. Bradl, Heavy Metals in the Environment: Origin, Interaction and Remediation, Vol. 6, Academic Press, London, 2002.
[3] R.C. Pena, A.P.R. de Souza, M. Bertotti, Determination of Fe (III) in wine samples using a ruthenium oxide hexacyanoferrate modified microelectrode, J. Electroanal. Chem., 731 (2014) 49–52.
[4] N. Abbaspour, R. Hurrell, R. Kelishadi, Review on iron and its importance for human health, J. Res. Med. Sci., 19 (2014) 164–174.
[5] M.T. Nunez, V. Tapia, S. Toyokuni, S. Okada, Iron-induced oxidative damage in colon carcinoma (Caco-2) cells, Free Radic. Res., 34 (2001) 57–68.
[6] S.M. Abdel-Azeem, N.R. Bader, H.M. Kuss, M.F. El-Shahat, Determination of total iron in food samples after flow injection preconcentration on polyurethane foam functionalized with N,N-bis(salicylidene)-1,3-propanediamine, Food Chem., 138 (2013) 1641–1647.
[7] C. Niederau, R. Fischer, A. Purschel, W. Stremmel, D. Haussinger, Longterm survival in patients with hereditary hemochromatosis. Gastroenterology, 110 (1996) 1107–1119.
[8] H. Abdolmohammad-Zadeh, M. Galeh-Assadi, S. Shabkhizan, H. Mousazadeh, Sol–gel processed pyridinium ionic liquid-modified silica as a new sorbent for separation and quantification of iron in water samples, Arab. J. Chem., 9 (2016) S587–S594.
[9] M.A. Kassem, A.S. Amin, Spectrophotometric determination of iron in environmental and food samples using solid phase extraction, Food Chem., 141 (2013) 1941–1946.
[10] A. Asan, R. Aydin, D. Karsli Semiz, V. Erci, I. Isildak, A very sensitive flow-injection spectrophotometric determination method for iron (II) and total iron using 2′, 3, 4′, 5, 7-pentahydroxyflavone, Environ. Monit. Assess., 185 (2013) 2115–2121.
[11] B. Horstkotte, P. Chocholouš, P. Solich, Large volume preconcentration and determination of nanomolar concentrations of iron in seawater using a renewable cellulose 8-hydroquinoline sorbent microcolumn and universal approach of post-column eluate utilization in a Lab-on-Valve system, Talanta, 150 (2016) 213–223.
[12] A.S. Amin, A.A. Gouda, Utility of solid-phase spectrophotometry for determination of dissolved iron(II) and iron(III) using 2,3-dichloro-6-(3-carboxy-2-hydroxy-1-naphthylazo) quinoxaline, Talanta, 76 (2008) 1241–1245.
[13] A. Babaei, M. Babazadeh, E. Shams, Simultaneous determination of iron, copper, and cadmium by adsorptive stripping voltammetry in the presence of thymol phthalexone, Electroanalysis, 19 (2007) 978–985.
[14] M. Grotti, F. Soggia, F. Ardini, R. Frache, Determination of sub-nanomolar levels of iron in sea-water using reaction cell inductively coupled plasma mass spectrometry after $Mg(OH)_2$ coprecipitation, J. Anal. At. Spectrom., 24 (2009) 522–527.
[15] R. Mirzajani, N. Pourreza, A.R. Kiasat & Rezvan Abdollahzadeh, Solid phase extraction and determination of Fe (III) in some vegetables and natural water samples using a new inorganic/organic hybrid adsorbent, Int. J. Environ. Anal. Chem., 94 (2014) 411–426.
[16] S.G. Silva, P.V. Oliveira, F.R.P. Rocha, A green analytical procedure for determination of copper and iron in plant materials after cloud point extraction, J. Braz. Chem. Soc., 21 (2010) 234–239.
[17] H. Kaasalainen, A. Stefánsson, G.K. Druschel, Determination of Fe(II), Fe(III) and Fe_{total} in thermal water by ion chromatography spectrophotometry (IC-Vis), Int. J. Environ. Anal. Chem., 96 (2016) 1074–1090.
[18] Y. Ji, X. Liu, M. Guan, Ch. Zhao, H. Huang, H. Zhang, C. Wang, Preparation of functionalized magnetic nanoparticulate sorbents for rapid extraction of biphenolic pollutants from environmental samples, J. Sep. Sci., 32 (2009) 2139–2145.
[19] J.E. Smith, L. Wang, W.H. Tan, Bioconjugated silica-coated nanoparticles for bioseparation and bioanalysis, Trends Anal. Chem., 25 (2006) 848–855.
[20] A. Bavili Tabrizi, M.R. Rashidi, H. Ostadi, A Nanoparticle-based solid-phase extraction procedure followed by spectrofluorimetry to determine carbaryl in different water samples, J. Braz. Chem. Soc., 25 (2014) 709–715.
[21] T. Kamal, Sh. Bahadar Khan, A.M. Asiri, Synthesis of zero-valent Cu nanoparticles in the chitosan coating layer on cellulose microfibers: evaluation of azo dyes catalytic reduction, Cellulose, 23 (2016) 1911–1923.
[22] J.S. Yamania, S.M. Miller, M.L. Spaulding, J.B. Zimmerman, Enhanced arsenic removal using mixed metal oxide impregnated chitosan beads, Water Res., 46 (2012) 4427–4434.
[23] R.B.N. Baig, R.S. Varma, Magnetically retrievable catalysts for organic synthesis, Chem. Commun., 49 (2013) 752–770.
[24] W.L. Tan, N.H.H. Abu Bakar, M. Abu Bakar, Catalytic reduction of p-nitrophenol using chitosan stabilized copper nanoparticles, Catal. Lett., 145 (2015) 1626–1633.
[25] Y.A. Azarova, A.V. Pestov, S. Yu. Bratskaya, Application of chitosan and its derivatives for solid-phase extraction of metal and metalloid ions: a mini-review, Cellulose, 23 (2016) 2273–2289.

[26] A.A. Galhoum, A.A. Atia, M.G. Mahfouz, S.T. Abdel-Rehem, N.A. Gomaa, T. Vincent, E. Guibal, Dy(III) recovery from dilute solutions using magnetic-chitosan nano-based particles grafted with amino acids, J. Mater. Sci., 50 (2015) 2832–2848.
[27] J.D. Merrifield, W.G. Davids, J.D. MacRae, A. Amirbahman, Uptake of mercury by thiol-grafted chitosan gel beads, Water Res., 38 (2004) 3132–3138.
[28] R. Qu, Ch. Sun, M. Wang, Ch. Ji, Q. Xu, Y. Zhang, Ch. Wang, H. Chen, P. Yin, Adsorption of Au (III) from aqueous solution using cotton fiber/chitosan composite adsorbents, Hydrometallurgy, 100 (2009) 65–71.
[29] J. Xu, G. Yuvaraja, W. Zhang, Application of chitosan/poly(vinyl alcohol)/CuO (CS/PVA/CuO) beads as an adsorbent material for the removal of Pb(II) from aqueous environment, Colloids. Surf., *B*, 149 (2017) 184–195.
[30] J. Guijuan, B. Weiwei, G. Guimei, A.N. Baichao, Z. Haifeng, G. Shucai, Removal of Cu (II) from aqueous solution using a novel crosslinked alumina-chitosan hybrid adsorbent, Chin. J. Chem. Eng., 20 (2012) 641–648.
[31] P.K. Dutta, R. Srivastava, J. Dutta, Functionalized nanoparticles and chitosan-based functional nanomaterials, Adv. Polym. Sci., 254 (2013) 1–50.
[32] H. Zhu, L. Xiao, R. Jiang, G.M. Zeng, L. Liu, Efficient decolorization of azo dye solution by visible light-induced photocatalytic process using SnO_2/ZnO heterojunction immobilized in chitosan matrix, *Chem. Eng. J.*, 172 (2011) 746–753.
[33] R. Saravanan, E. Sacari, F. Gracia, M. Mansoob Khan, E. Mosquera, Conducting PANI stimulated ZnO system for visible light photocatalytic degradation of coloured dyes, J. Mol. Liq., 221 (2016) 1029–1033.
[34] D. Chen, X. Sun, Y. Guo, L. Qiao, X. Wang, Acetylcholinesterase biosensor based on multi-walled carbon nanotubes-SnO_2-chitosan nanocomposite, Bioprocess Biosyst. Eng., 38 (2015) 315–321.
[35] V. Kumar Gupta, R. Saravanan, S. Agarwal, F. Gracia, M. Mansoob Khan, J. Qin, R.V. Mangalaraja, Degradation of azo dyes under different wavelengths of UV light with chitosan-SnO2 nanocomposites, J. Mol. Liq., 232 (2017) 423–430.
[36] T. Yang, X. Guo, Y. Ma, Q. Li, L. Zhong, K. Jiao, Electrochemical impedimetric DNA sensing based on multi-walled carbon nanotubes–SnO_2–chitosan nanocomposite, Colloids Surf., B, 107 (2013) 257–261.
[37] A. Rajbhandari, T. Subedi, *Spectrophotometric Determination of Total Iron in Rice and Maize Samples*, Scientific World, Vol. 11, 2013, pp. 101–104.
[38] R. Mirzajani, N. Pourreza, S. Safar Ali Najjar, b-Cyclodextrin-based polyurethane (b-CDPU) polymers as solid media for adsorption and determination of Pb(II) ions in dust and water samples, Res. Chem. Intermed., 40 (2014) 2667–2679.
[39] R.B. Biniwale, N.S. Milmile, J.V. Pande, S. Karmakar, A. Bansiwal, T. Chakrabarti, Equilibrium isotherm and kinetic modeling of the adsorption of nitrates by anion exchange Indion NSSR resin, Desalination, 276 (2011) 38–44.
[40] S. Tazikeh, A. Akbari, A. Talebi, E. Talebi, Synthesis and characterization of tin oxide nanoparticles via the co-precipitation method, Mater. Sci.-Poland, 32 (2014) 98–101.
[41] Y. Haldorai, D. Kharismadewi, D. Tuma, J. Jin Shim, Properties of chitosan/magnetite nanoparticles composites for efficient dye adsorption and antibacterial agent, Korean J. Chem. Eng., 32 (2015) 1688–1693.
[42] Sh. Yang, Zh. Wu, L.P. Huang, B. Zhou, M. Lei, L. Sun, Q. Tian, J. Pan, W. Wu, H. Zhang, Significantly enhanced dye removal performance of hollow tin oxide nanoparticles via carbon coating in dark environment and study of its mechanism, Nanoscale Res. Lett., 9 (2014) 442–450.
[43] J. Xu, M. Chen, Ch. Zhang, Zh. Yi, Adsorption of uranium(VI) from aqueous solution by diethylenetriamine-functionalized magnetic chitosan, J. Radioanal. Nucl. Chem., 298 (2013) 1375–1383.
[44] J. Xu, L. Zhou, Y. Jia, Zh. Liu, A.A. Adesina, Adsorption of thorium (IV) ions from aqueous solution by magnetic chitosan resins modified with triethylene-tetramine, J. Radioanal. Nucl. Chem., 303 (2015) 347–356.
[45] W. Feng, D. Nansheng, Photochemistry of hydrolytic iron (III) species and photoinduced degradation of organic compounds, a mini review, Chemosphere, 41 (2000) 1137–1147.
[46] J. Fenga, X. Hea, X. Liub, X. Suna, Y. Lia, Preparation of magnetic graphene/mesoporous silica composites with phenyl-functionalized pore-walls as the restricted access matrix solid phase extraction adsorbent for the rapid extraction of parabens from water-based skin toners, J. Chromatogr. A, 1465 (2016) 20–29.
[47] K.Y. Kumar, T.N.V. Raj, S. Archana, S.B.B. Prasad, Sh. Olivera, H.B. Muralidhara, SnO_2 nanoparticles as effective adsorbents for the removal of cadmium and lead from aqueous solution: adsorption mechanism and kinetic studies, J. Water Process Eng., 13 (2016) 44–52.
[48] J. Daia, H. Yang, H. Yan, Y. Shangguan, Q. Zheng, R. Cheng, Phosphate adsorption from aqueous solutions by disused adsorbents: chitosan hydrogel beads after the removal of copper(II), Chem. Eng. J., 166 (2011) 970–977.
[49] Y. Ren, H.A. Abbood, F. He, Hong Peng, K. Huang, Magnetic EDTA-modified chitosan/SiO_2/Fe_3O_4 adsorbent: preparation, characterization, and application in heavy metal adsorption, Chem. Eng. J., 226 (2013) 300–311.
[50] Y.M. Hao, C. Man, Z.B. Hu, Effective removal of Cu (II) ions from aqueous solution by amino-functionalized magnetic nanoparticles, J. Hazard. Mater., 184 (2010) 392–399.
[51] M.K. Kim, K. Sh. Sundaram, G.A. Iyengar, K.P. Lee, A novel chitosan functional gel included with multiwall carbon nanotube and substituted polyaniline as adsorbent for efficient removal of chromium ion, Chem. Eng. J., 267 (2015) 51–64.
[52] M. Naushad, T. Ahamad, G. Sharma, A. Al-Muhtaseb, A.B. Albadarin, M.M. Alam, Z.A. ALOthman, S.M. Alshehri, A.A. Ghfar, Synthesis and characterization of a new starch/SnO_2 nanocomposite for efficient adsorption of toxic Hg^{2+} metal ion, Chem. Eng. J., 300 (2016) 306–316.
[53] A.U. Itodo, H.U. Itodo, Sorption energies Estimation Using Dubinin-Radushkevich and Temkin adsorption isotherms, Life Sci. J., 7 (2010) 33–39.
[54] M.J. Horsfall, A.I. Spiff, A.A. Abia, Studies on the influence of mercaptoacetic acid (MAA) modification of cassava (*Manihot sculenta* Cranz.) waste biomass on the adsorption of Cu^{2+} and Cd^{2+} from aqueous solution, Bull. Korean Chem. Soc., 25 (2004) 969–976.
[55] T. Fan, Y. Liu, B. Feng, G. Zeng, C. Yang, M. Zhou, H. Zhou, Z. Tan, X. Wang, Biosorption of cadmium (II), zinc (II) and lead (II) by *Penicillium simplicissimum*: isotherms, kinetics and thermodynamics, J. Hazard. Mater., 160 (2008) 661–665.
[56] J.N. *Miller*, J.C. *Miller*, *Statistics* and Chemometrics for Analytical Chemistry, 6th edn., Pearson Education Limited, England, London, 2010.
[57] B. Tanhaei, A. Ayati, M. Lahtinen, M. Sillanpa, Preparation and characterization of a novel chitosan/Al_2O_3/magnetite nanoparticles composite adsorbent for kinetic, thermodynamic and isotherm studies of Methyl Orange adsorption, Chem. Eng. J., 259 (2015) 1–10.
[58] R. Mirzajani, F. Kardani, Fabrication of ciprofloxacin molecular imprinted polymer coating on a stainless steel wire as a selective solid-phase microextraction fiber for sensitive determination of fluoroquinolones in biological fluids and tablet formulation using HPLC-UV detection, J. Pharm. Biomed. Anal., 122 (2016) 98–109.
[59] B. Peng, Y. Shen, Zh. Gao, M. Zhou, Y. Ma, Sh. Zhao, Determination of total iron in water and foods by dispersive liquid–liquid microextraction coupled with microvolume UV–vis spectrophotometry, Food Chem., 176 (2015) 288–293.